

Gate voltage controlled electronic transport through a ferromagnet/normal/ferromagnet junction on the surface of a topological insulator

Kun-Hua Zhang,¹ Zheng-Chuan Wang,¹ Qing-Rong Zheng,^{1,*} and Gang Su^{1,†}

¹*Theoretical Condensed Matter Physics and Computational Materials Physics Laboratory, School of Physics, University of Chinese Academy of Sciences, Beijing 100049, China*

We investigate the electronic transport properties of a ferromagnet/normal/ferromagnet junction on the surface of a topological insulator with a gate voltage exerted on the normal segment. It is found that the conductance oscillates with the width of normal segment and gate voltage, and the maximum of conductance gradually decreases while the minimum of conductance approaches zero as the width increases. The conductance can be controlled by tuning the gate voltage like a spin field-effect transistor. It is found that the magnetoresistance ratio can be very large, and can also be negative owing to the anomalous transport. In addition, when there exists a magnetization component in the surface plane, it is shown that only the component parallel to the junction interface has an influence on the conductance.

PACS numbers: 72.25.Dc, 73.20.-r, 73.23.Ad, 85.75.-d

I. INTRODUCTION

Topological insulators are new quantum states discovered recently, which have a bulk band gap and gapless edge states or metallic surface states due to the time-reversal-symmetry and spin-orbit coupling interaction¹. The two-dimensional (2D) topological insulator has first been predicted theoretically as a quantum spin Hall state^{2,3} and then observed experimentally⁴. The topological characterization of quantum spin Hall insulators can be generalized from 2D to three-dimensional (3D) case, and leads to the discovery of 3D topological insulator (TI)⁵⁻⁸. The TIs in 3D are usually classified according to the number of Dirac cones on their surfaces. Those strong topological insulators with odd number of Dirac cones on their surfaces are robust against the time-reversal invariant disorder, while the weak topological insulator is referred to those with even number Dirac cones on their surfaces which depends on the surface direction and might be broken even without breaking the time reversal symmetry^{5,8}. When the TIs are coated with magnetic or superconducting layers, the surface states could be gapped and many interesting properties emerge, such as half-integer quantum Hall effect⁹, Majorana fermion¹⁰, etc.

The topological surface states had been observed by several experimental groups by means of angle-resolved photoemission spectroscopy (ARPES)¹¹⁻¹³ and scanning tunneling microscopy (STM)^{14,15}. Although the residual bulk carrier density brings much difficulty to the surface states transport experiments^{16,17}, the signatures of negligible bulk carriers contributing to the transport¹⁸ and near 100% surface transport in topological insulator¹⁹ have been found recently in experiments.

The low energy physics of the surface states of strong topological insulators can be described by the 2D massless Dirac theory⁷, which is different from that in graphene where the spinors are composed of different sublattices²⁰. The topological surface states show strong

spin-orbit coupling, which may be applied to the spin field-effect transistors in spintronics²¹⁻²⁶. The electronic transport properties on topological insulator surface with magnetization has attracted a lot of attention²⁷⁻³⁴. In Refs. 27 and 28 the results are given in the limit of thin barrier (i.e., the width of barrier $L \rightarrow 0$ and barrier potential $V_0 \rightarrow \infty$ while $V_0 L$ is constant), and the physical origin of this thin barrier is the mismatch effect and built-in electric field of junction interface. Refs. 29 and 33 studied the spin valve on the surface of topological insulator, in which the exchange fields in the two ferromagnetic leads are assumed to align along the y axis direction. Refs. 30, 31, 32 and 34 investigated the electron transport through ferromagnetic barrier on the surface of a topological insulator. It is noted that both the electric potential barrier and the ferromagnetic barrier are the transport channels in these models. The bulk band gap of topological insulator is usually about 20-300 meV^{7,11-13,18}, in order to keep the transport at the Fermi energy inside the bulk gap, and the gate voltage on topological insulator should be finite.

In this paper, we study the electronic transport through a 2D ferromagnet/normal/ferromagnet junction on the surface of a strong topological insulator where a gate voltage is exerted on the normal segment with a finite width, and the exchange fields in the two ferromagnetic leads point mainly to the z axis direction. So far such a system has not been well studied. We find that the conductance oscillates with the width of normal segment and gate voltage, and the maximum of conductance gradually decreases while the minimum of conductance can approach zero as the width increases. These behaviors are more obvious when the gate voltage is smaller than the Fermi energy. This gate-controlled 2D topological ferromagnet/normal/ferromagnet junction shows the property of a spin field-effect transistor. The magnetoresistance (MR) can be very large and could also be negative owing to the anomalous transport. In addition, when there exists a magnetization component in the 2D plane, it is shown that only the magnetization compo-

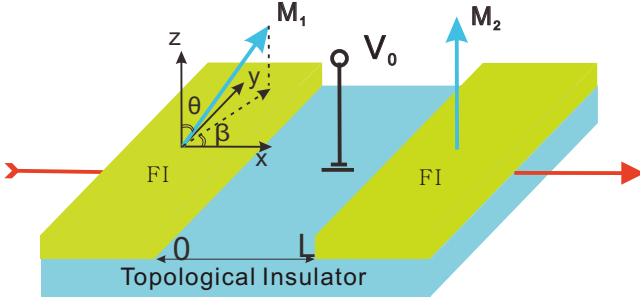


FIG. 1: (Color online) Schematic layout of a 2D ferromagnet/normal/ferromagnet junction on the surface of a topological insulator. An exchange split on the surface underneath the ferromagnetic insulator (FI) is induced by the proximity effect, and the central normal segment is tuned by a gate voltage V_0 . The current flows along the x-axis on the surface.

nent which is parallel to the junction interface has an influence on the conductance.

This paper is organized as follows. First, we will describe the theoretical model for the electronic transport through the topological spin-valve junction. Second, we will present our numerical results and discussions. Finally, a brief summary will be given.

II. THEORETICAL FORMALISM

We consider a 2D ferromagnet/normal/ferromagnet junction on a strong topological insulator surface as shown in Fig. 1. The bulk ferromagnetic insulator (FI) interacts with the surface electrons in TI by the proximity effect, and the ferromagnetism is induced in the topological surface states^{27–30,32,34,38–40}. The interfaces between ferromagnet (FM) and normal segment are parallel to y direction, and the normal segment is located between $x = 0$ and $x = L$ with gate voltage V_0 exerted on it^{35–37}. Here we presume, for the simplicity, the distance L between two interfaces is shorter than the mean free path as well as the spin coherence length. With this setup, the Hamiltonian for this system reads^{27–30,32,34}

$$\hat{H} = v_F \hat{\sigma} \cdot \hat{p} + \hat{\sigma} \cdot \vec{m}(r) + V(r) \quad (1)$$

with Pauli matrices $\hat{\sigma} = (\hat{\sigma}_x, \hat{\sigma}_y, \hat{\sigma}_z)$, the in-plane electron momentum $\hat{p} = (\hat{p}_x, \hat{p}_y, 0)$, and Fermi velocity v_F . The piecewise magnetization $\vec{m}(r)$ is chosen to be a 3D vector pointing along an arbitrary direction in the left region with $\vec{m}_L = (m_{Lx}, m_{Ly}, m_{Lz}) = m_L(\sin \theta \cos \beta, \sin \theta \sin \beta, \cos \theta)$, and fixed along the z axis perpendicular to the TI surface in the right region with $\vec{m}_R = (0, 0, m_{Rz})$. We can use a soft magnetic insulator for the left ferromagnet, which is controlled by a weak external magnetic field, and a magnetic insulator with very strong easy-axis anisotropy for the right ferromagnet. The configuration between the left and right ferromagnets directly depends on the weak external mag-

netic field, where the interlayer (RKKY) exchange coupling between left and right ferromagnets⁴¹ is ignored for the simplicity. In the middle segment, there is no magnetization, but instead, a gate voltage V_0 is exerted.

Solving Eq.(1), we obtain the wave function in the left region as following:

$$\begin{aligned} \psi_L(x \leq 0) = & A \left(\frac{v_F \hbar k_x + m_{Lx} - i(v_F \hbar k_y + m_{Ly})}{E - m_{Lz}} \right) e^{ik_x x} \\ & + B \left(\frac{-(v_F \hbar k_x + m_{Lx}) - i(v_F \hbar k_y + m_{Ly})}{E - m_{Lz}} \right) e^{-i(k_x + \frac{2m_{Lx}}{v_F \hbar})x} \end{aligned} \quad (2)$$

where the Fermi energy lies in the upper bands of Dirac cone, and $E > 0$. We also define ϕ as the incident angle, then $k_x = (\sqrt{E^2 - m_{Lz}^2} \cos \phi - m_{Lx})/v_F \hbar$, $k_y = (\sqrt{E^2 - m_{Lz}^2} \sin \phi - m_{Ly})/v_F \hbar$. The wave function in normal region ψ_C depends on the gate voltage. If $V_0 \neq E$,

$$\begin{aligned} \psi_C(0 \leq x \leq L) = & C \left(\frac{v_F \hbar(k'_x - ik_y)}{E - V_0} \right) e^{ik'_x x} \\ & + D \left(\frac{-v_F \hbar(k'_x + ik_y)}{E - V_0} \right) e^{-ik'_x x} \end{aligned} \quad (3)$$

where $k'_x = \pm \sqrt{((E - V_0)/v_F \hbar)^2 - k_y^2}$ with the \pm corresponding to the upper bands and the lower bands of the Dirac cone respectively, and if $V_0 = E$,⁴² it becomes

$$\begin{aligned} \psi_C(0 \leq x \leq L) = & C \begin{pmatrix} 0 \\ 1 \end{pmatrix} e^{-k_y x} \\ & + D \begin{pmatrix} 1 \\ 0 \end{pmatrix} e^{k_y x} \end{aligned} \quad (4)$$

The wave function in the right region is:

$$\psi_R(L \leq x) = F \left(\frac{v_F \hbar(k''_x - ik_y)}{E - m_{Rz}} \right) e^{ik''_x x} \quad (5)$$

with $k''_x = \sqrt{(E^2 - m_{Rz}^2)/(v_F \hbar)^2 - k_y^2}$. There exists a translation invariance along the y direction, so the momentum k_y is conserved in the three regions, and we omit the part $e^{ik_y y}$ in wave functions. These piecewise wave functions are connected by the boundary conditions:

$$\psi_L(0) = \psi_C(0), \quad \psi_C(L) = \psi_R(L) \quad (6)$$

which determine the coefficients A, B, C, D and F in the wave functions.

As a result, according to the Landauer-Büttiker formula⁴³, it is straightforward to obtain the ballistic conductance G at zero temperature

$$G = \frac{e^2 w_y}{h \pi} \frac{E_F}{v_F \hbar} \frac{1}{2} \int_{-\frac{\pi}{2}}^{\frac{\pi}{2}} d\phi \frac{F^* F}{A^* A} \frac{(E_F - m_{Lz}) v_F \hbar k''_x}{(E_F - m_{Rz}) E_F} \quad (7)$$

where w_y is the width of interface along the y direction, which is much larger than L , and we take E as E_F , because in our case the electron transport happens around the Fermi level.

III. NUMERICAL RESULTS AND DISCUSSIONS

We focus on the two cases about the electronic transport controlled by a gate voltage through this 2D topological ferromagnet/normal/ferromagnet junction. One is the conductance G and the magnetoresistance when the magnetizations in the left and right FM are collinear in the z -direction, and another is the influence of the magnetization component along the x/y direction on the conductance.

A. The conductance and MR for collinear magnetization

We show the normalized conductance G/G_0 as a function of $k_F L$ and V_0/E_F of parallel (Fig. a and c) and antiparallel (Fig. b and d) configurations for two different magnetizations along the z -axis in Fig. 2, where $G_0 = \frac{e^2 w_y}{h\pi} \frac{E_F}{v_F \hbar}$. In Figs. 2(a) and 2(b) we choose $m_{Lz} = m_{Rz} = 0.95E_F$, while in Figs. 2(c) and 2(d) $m_{Lz} = m_{Rz} = 0.6E_F$. In Fig. 2(a) the gap of surface

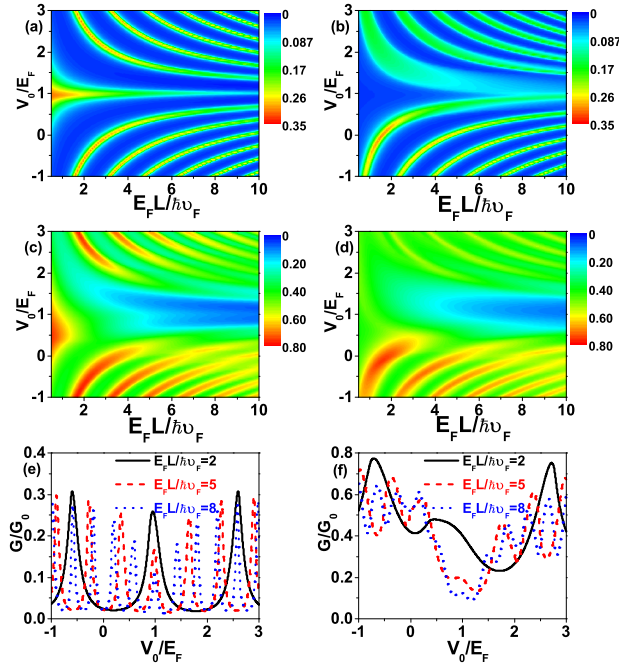


FIG. 2: (Color online) The normalized conductance G/G_0 as a function of $E_F L / v_F \hbar$ and V_0 / E_F , $m_{Lz} = m_{Rz} = 0.95E_F$ in (a) and (b), $m_{Lz} = m_{Rz} = 0.6E_F$ in (c) and (d). (a) and (c) correspond to the parallel configuration, (b) and (d) correspond to the antiparallel configuration. (e) and (f) are the sections of (a) and (c) for three $E_F L / v_F \hbar$'s respectively.

state in the left and right ferromagnet regions opened by the magnetization along the z -axis is $0.95E_F$. The

conductance oscillates with the gate voltage V_0 (parameters $E_F L / v_F \hbar$ and V_0 / E_F in Fig. 2 are dimensionless). The maximum of conductance gradually decreases as the width increases. The minimum of conductance can approach to zero. The change of conductance between maximum and minimum by gate voltage is similar to the spin field-effect transistor, in which the conductance modulation arises from the spin precession due to the spin-orbit coupling²¹. The gate voltage can be used to change the k'_x such that the phase factor $k'_x L$ of quantum interference in the normal segment can be changed. The oscillation period of conductance with respect to V_0 depends on the width L and decreases with the increase of width L . The conductance has a period π with respect to $z = V_0 L$, when $V_0 \rightarrow \infty, L \rightarrow 0$, in 2D topological ferromagnet/ferromagnet junction^{27,28}.

In Fig. 2(b), the conductance changes with the width L and gate voltage V_0 in the same way as in Fig. 2(a). The difference is that the conductance is maximum in Fig. 2(b) while it is minimum in Fig. 2(a) and vice versa. The conductance in Fig. 2(c) and Fig. 2(d) show the same variation tendency with the width L and gate voltage V_0 as Fig. 2(a) and Fig. 2(b), respectively. However both the maximum and minimum of conductance in Fig. 2(c) and Fig. 2(d) are larger than those in Fig. 2(a) and Fig. 2(b), since the gap of surface states in left and right ferromagnet regions is $0.6E_F$ in Fig. 2(c) and Fig. 2(d). The conductance changes more obviously with the gate voltage at the side of $V_0 / E_F < 1$ than at the side of $V_0 / E_F > 1$. In Fig. 2, both the maximum and minimum of the conductance become smaller when the gate voltage is closer to the Fermi energy, because the number of the incident wave functions transported through the normal segment by the evanescent waves (imaginary k'_x) becomes bigger. Fig. 2 shows that the conductance of this 2D topological ferromagnet/normal/ferromagnet junction could be changed by the same way as that in the spin field-effect transistor. While for the reason of the angular spectrum of electrons in the surface plane and the linear dispersion relation, how to get a large maximum/minimum ratio of the conductance is important for a transistor.

After obtaining the conductance G_P of parallel configuration and G_{AP} of antiparallel configuration, we can get the MR directly, which is defined as $MR = (G_P - G_{AP})/G_P$. Compared with the conductance in Fig. 2(a) and Fig. 2(c), the conductance in Fig. 2(b) and Fig. 2(d) shows a property indicated below. On the one hand, the conductance in the antiparallel configuration can be less than that in the parallel configuration as in the conventional spin valve²²⁻²⁴ and its counterpart in graphene⁴⁴. On the other hand, the conductance in the antiparallel configuration can also be larger than that in the parallel configuration, which is an anomalous electronic transport property of topological spin-valve junction. Fig. 3 shows the MR as a function of the width L . When $V_0 / E_F \neq 1$, the MR oscillates with the width L . The amplitude and period of oscillation of MR depend on the gate voltage

V_0 . When $V_0/E_F = 1$, the MR does not oscillate and decreases monotonically with the increase of L , because the Fermi surface of normal segment is at the Dirac point in this case and the corresponding density of states is zero while the conductance is not zero, which is a typical property of Dirac fermion system⁴². The MR could be negative for the anomalous electronic transport^{27,45}. The maximum of MR in Fig. 3(a) is larger than that in Fig. 3(b), and it can approach 100%. The big negative MR (more than -10) in Fig. 3(a) also means a big variation of conductance between parallel and antiparallel configuration.

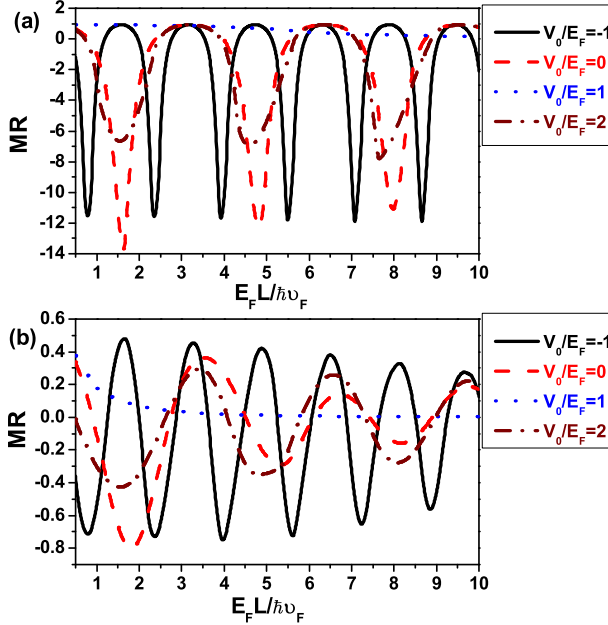


FIG. 3: (Color online) The MR as a function of the width $E_F L / \hbar v_F$ with different gate voltage V_0 . (a) $m_{Lz} = m_{Rz} = 0.95 E_F$; and (b) $m_{Lz} = m_{Rz} = 0.6 E_F$.

Next we will discuss the underlying physics quantitatively to understand the above results clearly. Since the electrons from all incident angles give contributions to the conductance which is proportional to the electron transmission probability, the physical origin of conductance oscillating with the width L and gate voltage V_0 in Fig. 2 is a direct result of summation of electron transmission probability over all incident angles.

Fig. 4 plots the transmission probability as a function of incident angle ϕ and width L for different gate voltage V_0 . We find that the transmission probability mainly oscillates with the width L . Its period of oscillation becomes large as the gate voltage increases from $V_0/E_F = 0$ to $V_0/E_F = 1$. The reason for such a change can be illustrated in Fig. 5. Because the wave functions in the left and right FMs are connected through the wave function in normal segment, the transmission probability

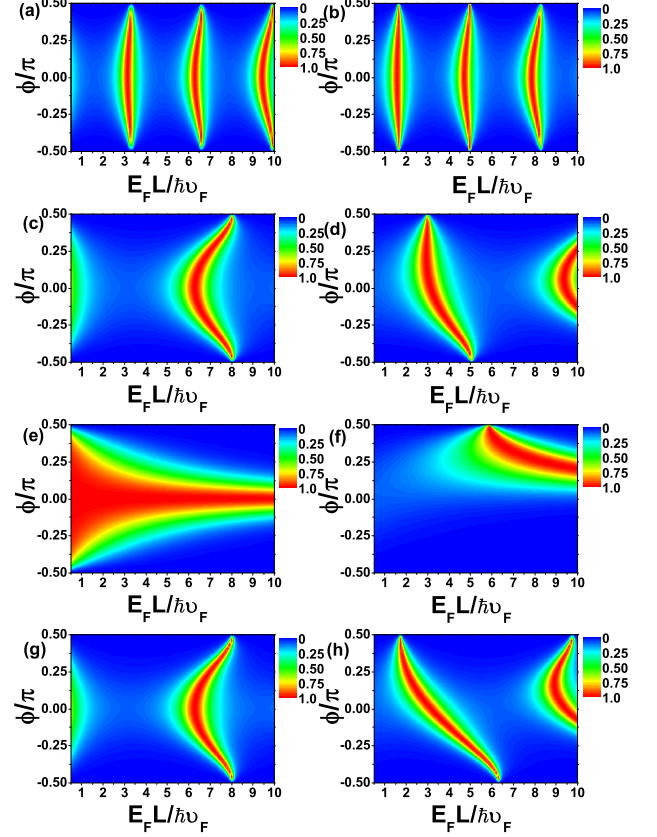


FIG. 4: (Color online) Transmission probability as a function of incident angle ϕ and width $E_F L / \hbar v_F$ where $m_{Lz} = m_{Rz} = 0.95 E_F$, we choose the parallel configuration at the left-hand side and the antiparallel configuration at the right-hand side, and the gate voltage V_0/E_F in (a) and (b), (c) and (d), (e) and (f), (g) and (h) are 0, 0.5, 1 and 1.5, respectively.

depends on the phase factor $k'_x L$. Due to the conservation of momentum k_y , k'_x depends on the gate voltage. When the gate voltage from $V_0/E_F = 0$ to 1, the Fermi surface for the normal region reduces as in Fig. 5, and k'_x reduces too, such that the transmission probability has a longer periodicity with the width L and changes considerably with incident angles as shown in Fig. 4(a) or 4(b) and 4(c) or 4(d). In these cases, the electronic transport through the normal segment occurs in the upper bands of Dirac cone. Although the Fermi surface for the normal segment in Fig. 4(g) or 4(h) is equal to that in Fig. 4(c) or 4(d), their transmission probability is different, because in Fig. 4(g) or 4(h) the electronic transport through the normal segment occurs in lower bands of Dirac cone. When the gate voltage $V_0/E_F = 1$, the electronic transport through the normal segment is totally due to the evanescent waves, the transmission probability is not a periodic function of width L as in Fig. 4(e) or 4(f).

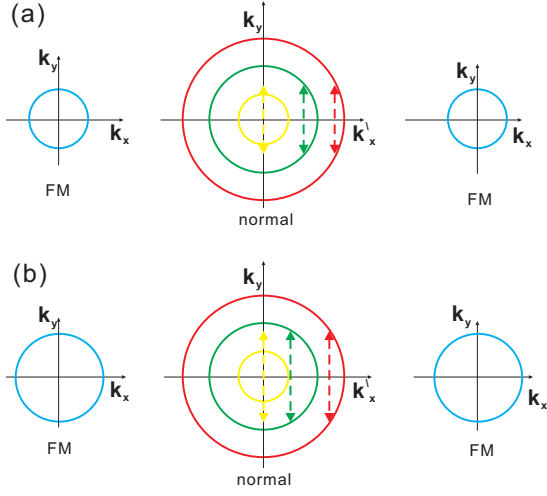


FIG. 5: (Color online) Fermi surfaces of the ferromagnet/normal/ferromagnet junction in momentum space, where the different colored Fermi surfaces in the normal segment stand for the cases with different gate voltages and the dashed lines have the same length which equals to the range of momentum k_y of incident wave function in (a) and (b), respectively. (a) $m_{Lz} = m_{Rz} = 0.95E_F$, and (b) $m_{Lz} = m_{Rz} = 0.6E_F$.

Now we consider the influence of magnetization configuration on the transmission probability. It is clearly that the transmission probability is an even function of the incident angle ϕ in the parallel configuration at the left-hand side of Fig. 4, while it is not an even function of the incident angle ϕ in the antiparallel configuration at the right-hand side. This is unusual, because the transmission probability is an even function of the incident angle ϕ on the antiparallel configuration in its counterpart in graphene⁴⁴. This unusual property arises from the unequal spinor parts of the incident and transmission wave functions. At the normal incidence ($\phi = 0$), the period of the transmission probability with the width L in the parallel configuration is the same as that in the antiparallel configuration and the position of maximum of the transmission probability has a shift of the half-period between two configurations. Now with the help of Figs. 4 and 5, the properties of conductance in Fig. 2(a) and 2(b) and MR in Fig. 3(a) could be understood explicitly.

When the magnetizations in the left and right FMs are taken as $0.6E_F$ in Fig. 5(b), one may see that the gaps of the surface states in the left and right ferromagnet regions decrease, and the Fermi surfaces in the left and right FMs become large. So, the range of k_y expands, and those of k'_x and the phase factor $k'_x L$ expand too. The transmission probability in Fig. 6 changes more dramatically than in Figs. 4(c) and 4(d), 4(g) and 4(h). Therefore, as the gap of surface states in left and right ferromagnet regions decreases, more incident electronic states will contribute to the conductance, such that the conductance becomes larger on the whole, and more unsymmetrical about the gate voltage $V_0/E_F = 1.0$ in Fig.

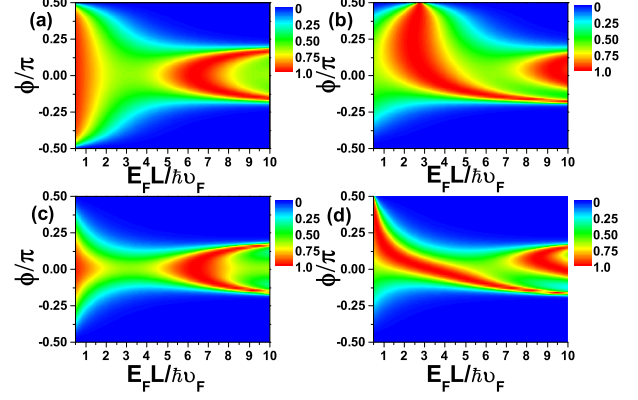


FIG. 6: (Color online) Transmission probability as a function of incident angle ϕ and the width $E_F L / \hbar v_F$, where $m_{Lz} = m_{Rz} = 0.6E_F$, and we choose the parallel configuration at the left-hand side and the antiparallel configuration at the right-hand side, and the gate voltage $V_0/E_F = 0.5$ and 1.5 in (a) and (b), (c) and (d), respectively.

2(c) and Fig. 2(d). The MR in Fig. 3(b) could be understood, similarly.

B. The influence of x/y component of magnetization on the conductance

Now we consider the influence of x/y component of magnetization on the conductance. First, we choose the z component of magnetization in the left and right FM to be equal as that in subsection A. We find that the influences of x/y component of magnetization on the conductance are quite different. The x component of magnetization has no influence on the conductance, while the y component of magnetization has a great influence on the conductance. Because the x component of magnetization just moves the Fermi surface along the x axis, the states contributing to the conductance do not change, while the y component of magnetization shifts the Fermi surface in the left FM along the y direction and decreases the number of incident electron states that contribute to the conductance. The influence of m_{Ly} on the conductance is shown in Fig. 7. It is seen that the conductance decreases with increasing $|m_{Ly}|$, so a large $|m_{Ly}|$ can lead the conductance to be zero. We also discover that the influence of magnetization m_{Ly} on the conductance is different from that of $-m_{Ly}$.

Second, by keeping the magnetizations in the left and right FMs the same value, the direction of magnetization in the left FM is changed in the x-z plane ($\beta = 0$) or in the y-z plane ($\beta = \pi/2$), where θ and β are indicated as shown in Fig. 1. The conductance as a function of θ and the gate voltage V_0 is plotted in Fig. 8, which is different from that in ferromag-

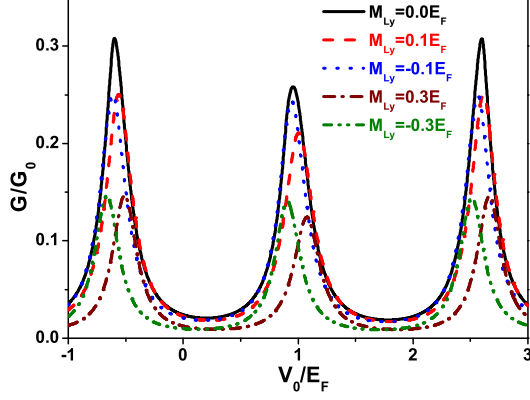


FIG. 7: (Color online) The conductance as a function of the gate voltage V_0 for different m_{Ly} , where $E_F L / \hbar v_F = 2$ and $m_{Lz} = m_{Rz} = 0.95E_F$.

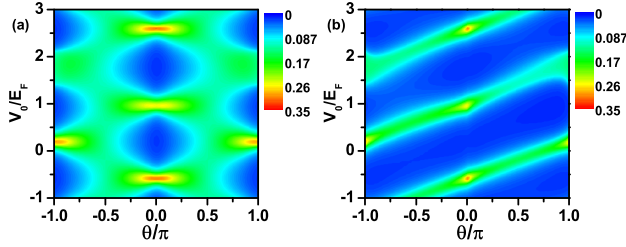


FIG. 8: (Color online) The conductance as a function of θ and gate voltage V_0/E_F for $E_F L / \hbar v_F = 2$, $m = |(m_{Lx}, m_{Ly}, m_{Lz})| = |(0, 0, m_{Rz})| = 0.95E_F$, the angle θ is (a) in the x-z plane ($\beta = 0$) and (b) in the y-z plane ($\beta = \pi/2$).

netic/normal/ferromagnetic graphene junction⁴⁵. The distinction between Figs. 8(a) and 8(b) is more obvious at $\theta = \pm 0.5\pi$, where the conductance changes slightly with the gate voltage in Fig. 8(a) while the conductance changes remarkably in Fig. 8(b). These results are from different connections of wave functions between left and right FMs. Since when $\theta = \pm 0.5\pi$, the spin in the right FM is parallel to $(v_F \hbar k_x^R, v_F \hbar k_y, m)^t$,²⁷ and the spin in the left FM is parallel to $(v_F \hbar k_{x1} \pm m, v_F \hbar k_{y1}, 0)^t$ in Fig. 8(a) which satisfies the relation $E = \sqrt{(v_F \hbar k_{x1} \pm m)^2 + (v_F \hbar k_{y1})^2}$, while the spin in the left FM is parallel to $(v_F \hbar k_{x2}, v_F \hbar k_{y2} \pm m, 0)^t$ in Fig. 8(b) which satisfies the relation $E = \sqrt{(v_F \hbar k_{x2})^2 + (v_F \hbar k_{y2} \pm m)^2}$. In this case, the z component of spin in the left FM is 0 in Figs. 8(a) and 8(b). Because in Fig. 8(b) the Fermi surface of left FM shifts along the y direction about $\pm m$, the difference of x component of spin between the left FM and right FM in Fig.

8(a) is larger than that in Fig. 8(b).

Finally, we discuss the realization of our model. The bulk band gap of topological insulator is small and depends on the materials, which is for example, about 300 meV in Bi_2Se_3 , 100 meV in Bi_2Te_3 ^{7,12,13}, and 22 meV in HgTe¹⁸. Far away from the Dirac point, the surface electronic states exhibit large deviations from the simple Dirac cone in Bi_2Te_3 ⁴⁶. The gap of surface states could be induced by putting the magnetic insulator on the surface of a topological insulator (such as EuO, EuS and MnSe). Depending on the interface match of the topological insulator and ferromagnetic insulator, the gap is several to dozens of meV^{27,38–40}. The gate electrode could be attached to the topological insulator to control the surface potential^{35–37}. The predicted properties of our model may be observed when the Fermi energy of surface states is about 10 – 100 meV, and the junction width is about 10 – 100 nm. The calculated results in this paper are based on the ballistic transport. In order to observe experimentally our predicted properties, a clean 2D topological surface states with enough long mean free path is needed. It is interesting to note that the surface of topological insulator with such a long mean free path can be realized in experiments³⁶.

IV. SUMMARY

In summary, we have studied the electronic transport properties of the ferromagnet/normal/ferromagnet junction on the surface of a strong topological insulator, where a gate voltage is exerted on the normal segment with a finite width. It is found that the conductance oscillates with the width of normal segment and the gate voltage. The maximum of conductance gradually decreases as the width increases and the minimum of conductance approaches zero. This gate-controlled conductance behaves in the same way as the spin field-effect transistor does, but a further study is needed to increase the maximum/minimum ratio of the conductance. The magnetoresistance can be very large and could also be negative owing to the anomalous transport. In addition, when there exists a magnetization component in the 2D plane, it is shown that only the magnetization component parallel to the junction interface has an influence on the conductance.

Acknowledgments

One of authors (KHZ) acknowledges discussions with Fei Ye and Zhe Zhang. This work is supported in part by the NSFC (Grant Nos. 90922033, 10934008, and 10974253), the MOST of China (Grant No. 2012CB932900 and 2013CB933401) and the CAS.

-
- * Electronic address: qrzheng@ucas.ac.cn
† Electronic address: gsu@ucas.ac.cn
- ¹ M. Z. Hasan, and C. L. Kane, *Rev. Mod. Phys.* **82**, 3045 (2010); X. L. Qi, and S. C. Zhang, *ibid.*, **83**, 1057 (2011).
 - ² C. L. Kane, and E. J. Mele, *Phys. Rev. Lett.* **95**, 146802 (2005); **95**, 226801 (2005).
 - ³ B. A. Bernevig, T. L. Hughes, and S. C. Zhang, *Science* **314**, 1757 (2006).
 - ⁴ M. König, S. Wiedmann, C. Brüne, A. Roth, H. Buhmann, L. W. Molenkamp, X. L. Qi, and S. C. Zhang, *Science* **318**, 766 (2007).
 - ⁵ L. Fu, C. L. Kane, and E. J. Mele, *Phys. Rev. Lett.* **98**, 106803 (2007).
 - ⁶ R. Roy, *Phys. Rev. B* **79**, 195322 (2009); J. E. Moore, and L. Balents, *ibid.*, **75**, 121306(R) (2007).
 - ⁷ H. Zhang, C. X. Liu, X. L. Qi, X. Dai, Z. Fang, and S. C. Zhang, *Nat. Phys.* **5**, 438 (2009).
 - ⁸ L. Fu, and C. L. Kane, *Phys. Rev. B* **76**, 045302 (2007).
 - ⁹ Y. Zheng, and T. Ando, *Phys. Rev. B* **65**, 245420 (2002).
 - ¹⁰ L. Fu, and C. L. Kane, *Phys. Rev. Lett.* **100**, 096407 (2008).
 - ¹¹ D. Hsieh, D. Qian, L. Wray, Y. Xia, Y. S. Hor, R. J. Cava, and M. Z. Hasan, *Nature* **452**, 970 (2008).
 - ¹² Y. Xia, D. Qian, D. Hsieh, L. Wray, A. Pal, H. Lin, A. Bansil, D. Grauer, Y. S. Hor, R. J. Cava, and M. Z. Hasan, *Nat. Phys.* **5**, 398 (2009).
 - ¹³ Y. L. Chen, J. H. Chu, J. G. Analytis, Z. K. Liu, K. Igarashi, H. H. Kuo, X. L. Qi, S. K. Mo, R. G. Moore, D. H. Lu, M. Hashimoto, T. Sasagawa, S. C. Zhang, I. R. Fisher, Z. Hussain, and Z. X. Shen, *Science* (329) 659 (2010).
 - ¹⁴ T. Zhang, P. Cheng, X. Chen, J. F. Jia, X. Ma, K. He, L. Wang, H. Zang, X. Dai, Z. Fang, X. Xie, and Q. K. Xue, *Phys. Rev. Lett.* **103**, 266803 (2009).
 - ¹⁵ J. Seo, P. Roushan, H. Beidenkopf, Y. S. Hor, R. J. Cava, and A. Yazdani, *Nature* **466**, 343 (2010).
 - ¹⁶ J. G. Analytis, R. D. McDonald, S. C. Riggs, J. H. Chu, G. S. Boebinger, and I. R. Fisher, *Nat. Phys.* **6**, 960 (2010).
 - ¹⁷ K. Eto, Z. Ren, A. A. Taskin, K. Segawa, and Y. Ando, *Phys. Rev. B* **81**, 195309 (2010).
 - ¹⁸ C. Brüne, C. X. Liu, E. G. Novik, E. M. Hankiewicz, H. Buhmann, Y. L. Chen, X. L. Qi, Z. X. Shen, S. C. Zhang, and L. W. Molenkamp, *Phys. Rev. Lett.* **106**, 126803 (2011).
 - ¹⁹ B. Xia, M. Y. Liao, P. Ren, A. Sulaev, S. Chen, C. Soci, A. Huan, A. T. S. Wee, A. Rusydi, S. Q. Shen, and L. Wang, *arXiv*: **1203**. 2997.
 - ²⁰ C. W. J. Beenakker, *Rev. Mod. Phys.* **80**, 1337 (2008); A. H. Castro Neto, F. Guinea, N. M. R. Peres, K. S. Novoselov, and A. K. Geim, *Rev. Mod. Phys.* **81**, 109 (2009).
 - ²¹ S. Datta, and B. Das, *Appl. Phys. Lett.* **56**, 665 (1990).
 - ²² I. Žutić, J. Fabian, and S. Das. Sarma, *Rev. Mod. Phys.* **76**, 323 (2004).
 - ²³ S. A. Wolf, D. D. Awschalom, R. A. Buhrman, J. M. Daughton, S. von Molnár, M. L. Roukes, A. Y. Chtchelkanova, and D. M. Treger, *Science* **294**, 1488 (2001).
 - ²⁴ A. Fert, *Rev. Mod. Phys.* **80**, 1517 (2008).
 - ²⁵ Z. G. Zhu, G. Su, Q. R. Zheng, and B. Jin, *Phys. Rev. B* **68**, 224413 (2003); B. Jin, G. Su, Q. R. Zheng, and M. Suzuki, *Phys. Rev. B* **68**, 144504 (2003).
 - ²⁶ H. F. Mu, Q. R. Zheng, B. Jin, and G. Su, *Phys. Lett. A* **336**, 66 (2005); H. F. Mu, G. Su, and Q. R. Zheng, *Phys. Rev. B* **73**, 054414 (2006); X. Chen, Q. R. Zheng, and G. Su, *Phys. Rev. B* **78**, 104401 (2008).
 - ²⁷ T. Yokoyama, Y. Tanaka, and N. Nagaosa, *Phys. Rev. B* **81**, 121401(R) (2010).
 - ²⁸ B. Soodchomshom, *Phys. Lett. A* **374**, 2894 (2010).
 - ²⁹ M. Salehi, M. Alidoust, Y. Rahnavard, and G. Rashedi, *Phys. E* **43**, 966 (2011).
 - ³⁰ S. Mondal, D. Sen, K. Sengupta, and R. Shankar, *Phys. Rev. Lett.* **104**, 046403 (2010); S. Mondal, D. Sen, K. Sengupta, and R. Shankar, *Phys. Rev. B* **82**, 045120 (2010).
 - ³¹ Jinhua Gao, Wei-Qiang Chen, Xiao-Yong Feng, X. C. Xie, and Fu-Chun Zhang, *arXiv*: **0909**. 0378v1.
 - ³² J. P. Zhang, and J. H. Yuan, *Eur. Phys. J. B* **85**, 100 (2012).
 - ³³ Jian-Hui Yuan, Ze Cheng, Jian-Jun Zhang, Qi-Jun Zeng, and Jun-Pei Zhang, *arXiv*: **1204**. 0956v1.
 - ³⁴ Z. Wu, F. M. Peeters, and K. Chang, *Phys. Rev. B* **82**, 115211 (2010); Y. Zhang, and F. Zhai, *Appl. Phys. Lett.* **96**, 172109 (2010).
 - ³⁵ H. Steinberg, J. B. Laloë, V. Fatemi, J. S. Moodera, and P. Jarillo-Herrero, *Phys. Rev. B* **84**, 233101 (2011).
 - ³⁶ Y. Wang, F. Xiu, L. Cheng, L. He, M. Liang, J. Tang, X. Kou, X. Yu, X. Jiang, Z. Chen, J. Zou, and K. L. Wang, *Nano Lett.* **12**, 1170 (2012).
 - ³⁷ J. R. Williams, L. DiCarlo, and C. M. Marcus, *Science* **317**, 638 (2007).
 - ³⁸ H. Haugen, D. Huertas, and A. Brataas, *Phys. Rev. B* **77**, 115406 (2008).
 - ³⁹ I. Vobornik, U. Manju, J. Fujii, F. Borgatti, P. Torelli, D. Krizmancic, Y. S. Hor, R. J. Cava, and G. Panaccione, *Nano Lett.* **11**, 4079 (2011).
 - ⁴⁰ Weidong Luo, and Xiao-Liang Qi, *arXiv*: **1208**. 4638v1.
 - ⁴¹ I. Garate, and M. Franz, *Phys. Rev. B* **81**, 172408 (2010).
 - ⁴² M. I. Katsnelson, *Eur. Phys. J. B* **51**, 157 (2006).
 - ⁴³ S. Datta, *Electronic Transport in Mesoscopic Systems* (Cambridge University Press, Cambridge, 1995).
 - ⁴⁴ C. Bai, and X. Zhang, *Phys. Lett. A* **372**, 725 (2008).
 - ⁴⁵ T. Yokoyama, and J. Linder, *Phys. Rev. B* **83**, 081418(R) (2011).
 - ⁴⁶ Y. L. Chen, J. G. Analytis, J. H. Chu, Z. K. Liu, S. K. Mo, X. L. Qi, H. J. Zhang, D. H. Lu, X. Dai, Z. Fang, S. C. Zhang, I. R. Fisher, Z. Hussain, and Z. X. Shen, *Science* **325**, 178 (2009).